IEEE Access
Multidisciplinary | Rapid Review | Open Access Journal

Received December 17, 2017, accepted February 2, 2018, date of publication February 13, 2018, date of current version March 13, 2018.

Digital Object Identifier 10.1109/ACCESS.2018.2805802

Performance of Tri-Band Multi-Polarized Array Antenna for 5G Mobile Base Station Adopting Polarization and Directivity Control

KORANY R. MAHMOUD [1,2] AND AHMED M. MONTASER [3]

[1]Department of Electronics, Communications, and Computers, Faculty of Engineering, Helwan University, Cairo 11795, Egypt
[2]National Telecommunications Regulatory Authority, Ministry of Communication and Information Technology, Giza 12577, Egypt
[3]Electrical Engineering Department, Sohag University, Sohag 82524, Egypt

Corresponding author: Korany R. Mahmoud (kurany_hameda@h-eng.helwan.edu.eg)

This work was supported by the National Telecommunication Regulatory Authority, Ministry of Communication and Information Technology, Egypt.

ABSTRACT In this paper, the performance of tri-band multi-polarized adaptive array antenna for 5G mobile base station is introduced adopting the polarization and directivity control. First, the design of multi-band circularly polarized antenna element at 28/38/48 GHz is presented. The measured results show that the designed antenna element has a reflection coefficient of less than −20 dB in the assigned frequency bands of 28/38/48 GHz with a realized antenna gain of 7.82 dB, 8.39 dB, and 7.73 dB, respectively. Based on the designed antenna element, a 32-element are distributed in an octagonal prism configuration is presented as possible candidates for the future 5G mmWave cellular networks. The antenna array performance is studied in terms of gain, radiation efficiency, return loss, and axial ratio for different scenarios, in addition, the metrics of total scan pattern and coverage efficiency are investigated. To optimize the antenna parameters and synthesizing multi-beam patterns, a modified version of hybrid gravitational search algorithm and particle swarm optimization algorithm is introduced. This enhancement has improved the global search ability and accelerates the convergence capability. The proposed array antenna achieved good $S_{11} < -20$ dB with high isolation between the array elements. Besides, an acceptable realized gain of 16.85 dB on average with a radiation efficiency of more than 82 % is obtained in the entire operation bands.

INDEX TERMS Beamforming, multi-polarized antenna, particle swarm optimization, gravitational search algorithm, 5G mobile station.

I. INTRODUCTION

Due to increased usage of smartphones, tablets, new wireless devices and the internet of things (IoT), the wireless data traffic projected to increase 10,000 fold within the next few years [1], [2]. To meet this ever increasing demand in capacity, new spectrum beyond sub-6 GHz frequencies has to be used. One promising path is the utilization of underused millimeter wave (mmWave) frequency spectrum for future 5G networks [3]–[7]. By their nature, those high frequencies provide much more bandwidth than the spectrum below 6 GHz that is currently being used for mobile communication. In the United States, the federal communications commission (FCC) recently published rules which opened up 10.85 GHz of spectrum for flexible use wireless broadband [8]. The rules create a new upper microwave flexible use service in the 28 GHz (27.5-28.35 GHz), 37 GHz (37-38.6 GHz) and 39 GHz (38.6-40 GHz) bands, and a new unlicensed band at 64-71 GHz. Moreover, the FCC also released a further notice of proposed rulemaking on the following new bands: 24 to 25, 32, 42, 48, 51, 70 and 80 GHz to dramatically increase the spectrum available for next generation services.

Compared to the current sub-6 GHz cellular networks, mmWave communications experience large path loss and more sensitivity to blockages due to its higher frequencies [9]. Fortunately, the small wavelengths of mmWave frequencies facilitate the use of a large number of antenna elements in a compact form factor to synthesize highly directional beams corresponding to large array gains for multi-gigabit-per-second data rates [10]. Beamforming in mmWave cellular systems facilitated by a large number of antennas at base stations (BSs) and/or user equipments (UEs) is essential to

achieve reasonable coverage range and high spectrum efficiency [11], [12]. In [13], Turgut and Gursoy investigate the potential benefits of the directional beamforming in mmWave cellular networks and show that by increasing the main lobe gain results in higher coverage performance probability.

It is clear that, beamforming systems have been widely deemed to improve the capacity, reduce the interference, increase data rates, and improve the performance of wireless mobile communication. However, in the case of using a single polarized antenna array, the characteristics deteriorate when the mobile terminals approach each other and the angle-of-arrival difference seen from the base station is less than the resolution allowed by the directivity. Therefore, an imperative need is appeared to realize adaptive array antennas with horizontal, vertical, and circular polarization capacity to enhance the mmWave transmission and reception efficiency [14], [15]. Furthermore, to avoid a polarization mismatch, desired antennas should be able to switch from two orthogonal polarizations or use both of the polarized signals simultaneously.

Consequently, the design of 8×8 patch antenna array with polarization and space diversity for the 5G cellular networks at 28 GHz is presented in [16]. The rectangular patch antenna element is designed to have dual linear polarization, therefore, the proposed array antenna has dual-orthogonal polarization with good polarization isolation and realized gain of 21 dBi. In [17], a dual-polarized wideband aperture antenna with a backed cavity implemented on PCB substrates operating in a mmWave band of 28-35 GHz is presented for MIMO applications in 5G mobile communication systems. Also, a 2x2 array setting is included, where the antenna elements demonstrated good element-to-element isolation better than 18 dB. A mmWave dual-polarized antenna subarray, together with filtering responses, is reported in [18] for 5G base stations. The proposed antenna subarray consists of four radiators in order to provide full integration and good precision. A maximum gain of 10.8 dBi is achieved, within an impedance bandwidth of about 530 MHz for S_{11} less than -10 dB. However, all these dual-polarized antennas have been designed to contain two feeding ports, corresponding to orthogonal polarizations of radiated fields. Recently, IBM and Ericsson announced the world's first reported Si mmWave phased array antenna module operating at 28 GHz [19]. The module consists of four monolithic microwave integrated circuits (MMICs) and 64 dual-polarized antennas for concurrent dual polarization operation and 1.4° beam-steering resolution for 5G communication.

In the future mmWave cellular network, an aggressive spatial reuse may be possible. Backhaul links, for example, may share the same mmWave spectrum, allowing rapid deployment and mesh-like connectivity with cooperation between base stations. Therefore, space division multiple access (SDMA) configuration based on directivity and polarization is proposed to increase the number of multiplicities. In such case, the mmWave base station (MBS) will monitor the mutual correlation between UEs during the reception

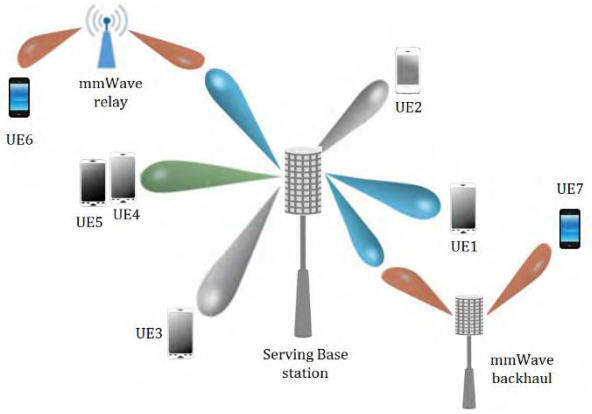

FIGURE 1. Illustration of a mmWave Base station communicate to users in cellular network.

mode and determines the polarization (vertical or horizontal) to be transmitted by each terminal in such a way that the mutual correlation between the terminals connected at the same time is minimized. Therefore, the base station in such configuration will have the ability to transmit vertically, horizontally, or circularly polarized (CP) according to the UE polarization status. As shown in Fig. 1, the MBS transmit simultaneously different beams to multiple directions with vertical polarization (e.g., UE1 and mmWave relay) and other UEs with horizontal polarization (e.g., UE2, and UE3) in the networks. However, when two UEs (e.g., UE4 and UE5) cannot be distinguished from one another by the MBS in angular domain, there are two beams transmitted (almost) in the same path with different polarization to each UE.

The mobile terminals in the proposed configuration will have the ability to transmit/receive vertically, horizontally, or circularly polarized waves according to the polarization control signal determined at the base station. In [20], a multi-polarized antenna array configuration for mobile phones is designed and verified at 28 GHz with wide beam scanning angle have been developed to enhance the transmission and reception efficiency. An innovative design of dual-band circularly polarized array antenna package for 5G mobile terminals with beam-steering capabilities is introduced in [21]. The proposed phased array antenna has good 3D beam-steering characteristics, which makes it suitable for mmwave 5G mobile applications.

To adaptively synthesize the BS beam pattern, a powerful optimization technique should be considered. In [22], Rashedi *et al.* have introduced the gravitational search algorithm (GSA) based on the law of gravity and the notion of mass interactions. Recently, a new hybrid population-based algorithm is proposed with the combination of particle swarm optimization PSO and GSA [23]. The main idea is to integrate the ability of exploitation in PSO with the ability of exploration in GSA to synthesize both algorithms' strength. For a variety of engineering design problems, the hybrid GSA-PSO algorithm showed a better capability to escape from local optimums with faster convergence than the standard

PSO and GSA [24]. The enhanced version of GSA-PSO is based on the idea of combining the ability of social thinking in law of gravity and mass interaction with the search capability of deterministic framework named Dynamic Threshold Optimization (DTO) [25], along with the addition of time-varying acceleration coefficients [26], to effectively control the global search and convergence to the global best solution.

To the best of the author's knowledge, there have been no systematic studies undertaken so far concerning multi-beam radiation patterns of 5G mmWave base station adopting directivity and polarization control at different frequency bands. Therefore, in this article, a multi-polarized antenna element is designed and verified at 28/38/48 GHz. Then, the antenna array in an octagonal prism arrangement is deployed at MBS to form multiple directional beams considering different scenarios. The optimal radiation patterns are developed based on a modified version of GSA-PSO (MGSA-PSO) technique by adjusting the excitation weight of each array element. The goal is to synthesize vertical and/or horizontal radiation beams toward the intended users or signals of interest (SOI) and ideally obtain nulls toward directions of interfering signals or signals not of interest (SNOI). Furthermore, the total scan pattern of the proposed array configuration together with its respective coverage efficiency are considered to analyze the performance of the 5G mmWave base station. In summary, the main contributions in this work are as follows:

- Firstly, a novel design of a tri-band CP antenna is presented at 28/38/48 GHz.
- Secondly, based on the designed antenna element, the beamforming capabilities of the considered array antenna for 5G mmWave base station is studied to form simultaneously multiple vertical (V)/horizontal (H) directional beams adopting the polarization and directivity control.
- Finally, a modified version of GSA-PSO algorithm is introduced as a powerful optimization technique to improve the convergence capability and decrease the required processing time.

The designed array antenna and optimization technique can be generalized to synthesize the beam-pattern for many scenarios. However, in this paper, only four different scenarios are considered to show the strength of the designed array antenna and the proposed technique.

In Section II, the modified GSA-PSO algorithm is introduced. The design and configuration of antenna element and base station array antenna are illustrated in Section III. The results are presented and discussed in Section IV. Finally, further discussions and conclusions are presented in Section V.

II. MODIFIED GSA-PSO ALGORITHM

In GSA, the position of each agent X_i provides a solution to the design problem. The mass value $M_i(t)$ of each agent i is determined according to its fitness value:

$$M_i(t) = \frac{q_i(t)}{\sum_{j=1}^{S} q_j(t)} \tag{1}$$

$$q_i(t) = \frac{fit_i(t) - worst(t)}{best(t) - worst(t)} \tag{2}$$

where $fit_i(t)$ represent the fitness value of the agent i at iteration t, worst(t) and best(t) are defined as follows:

$$best(t) = \max\ fit_j(t) \quad j \in \{1, \ldots, m\} \tag{3}$$

$$worst(t) = \min\ fit_j(t) \quad j \in \{1, \ldots, m\} \tag{4}$$

To evaluate the acceleration of an agent, total forces from a set of heavier masses applied on it should be considered based on law of gravity which is followed by law of motion to calculate the agent acceleration as follows:

$$a_i^d(t) = \frac{F_i^d(t)}{M_i(t)} = \sum_{j \neq i} rand_j\ G(t) \frac{M_j(t)}{R_{ij}(t) + \varepsilon} \left(x_j^d(t) - x_i^d(t)\right) \tag{5}$$

Where ε is a small value, $R_{ij}(t)$ is the Euclidean distance between two agents, i and j. G(t) is the universal gravitational constant and is defined as a function of time t:

$$G(t) = G_0 e^{\left(\frac{-\beta t}{t_{max}}\right)} \tag{6}$$

where G_0 is the initial value, β is a constant, t_{max} is the maximum number of iteration.

In the modified version of GSA-PSO algorithm, the time-varying acceleration coefficients $c_1(t)$ and $c_2(t)$ in addition to the time varying inertia weight, $\omega(t)$, are proposed to effectively control the global search and convergence towards the global best solution [26]. According to these modifications, the next velocity of an agent is calculated based on the ability of social thinking (gbest) in the PSO added to a fraction of its current velocity and its acceleration as in Eq. (7). Then, its next position can be calculated using the following equations, respectively:

$$v_i^d(t+1) = \omega(t)\, v_i^d(t) + c_1(t)\, rand_i\, a_i^d(t) + c_2(t)\, rand_j \left(gbest - x_i^d(t)\right) \tag{7}$$

$$x_i^d(t+1) = x_i^d(t) + v_i^d(t+1)\, \Delta t \tag{8}$$

where x_i^d, and v_i^d represent the position, and velocity of i-th agent in d-th dimension, respectively. $rand_i$ and $rand_j$ are uniform random variables in the interval [0, 1] to give a randomized characteristic to the search, gbest is the best solution so far and Δt is the unit time step.

The current inertia weight $\omega(t)$ is introduced to control the impact of the previous history of the velocities on the current velocity, thus to influence the trade-off between the global and local search abilities. The objective of this development is to enhance the global search during the early parts of the optimization and to encourage the agents to converge towards the global optima at the end of the search. In this development, the acceleration coefficients $c_1(t)$ and $c_2(t)$

TABLE 1. The values of the MGSA-PSO coefficients.

Coefficient	β	G_0	ω^{max}	ω^{min}	$c_1{}^{max}$	$c_1{}^{min}$	$c_2{}^{max}$	$c_2{}^{min}$	P	C_{th}
value	20	1	0.9	0.4	1.5	0.5	1.5	0.5	4	0.98

change with time. In each iteration t, the current weighting value and acceleration coefficients can be calculated using the following equations:

$$c_1(t) = c_1^{max} - \frac{c_1^{max} - c_1^{min}}{t_{max}} \times t \tag{9}$$

$$c_2(t) = c_2^{min} + \frac{c_2^{max} - c_2^{min}}{t_{max}} \times t \tag{10}$$

$$\omega(t) = \omega^{max} - \frac{\omega^{max} - \omega^{min}}{t_{max}} \times t \tag{11}$$

where, ω^{max} is the initial weight, ω^{min} is the final weight. By updating ω, c_1 and c_2 as depicted, the abilities of the global search and local search can be balanced. With a large cognitive component and a small social component at the beginning, the probes are allowed to move around the search space, instead of moving toward the population best. On the other hand, a small cognitive component and a large social component allow the probes to converge to the global optima in the later part of the optimization.

Furthermore, the decision space (DS) in the MGSA-PSO is adaptively compresses by the dynamic threshold optimization (DTO) that introduced in [25]. This approach based on compressing DS from below in the direction of the dependent variable using a series of successively increasing "thresholds," instead of shrinking DS. In DTO, the threshold value (T) is updated subsequently by applying the following auxiliary function:

$$g(\vec{x}) = \left[fit(\vec{x}) - T_{k-1}\right] \cdot U\left[fit(\vec{x}) - T_{k-1}\right] + T_{k-1} \tag{12}$$

where U[.] is the unit step function. Thus, for $fit(\vec{x}) \geq T$, $g(\vec{x}) = fit(\vec{x})$, whereas for $fit(\vec{x}) < T$, $g(\vec{x}) = T$. DTO was implemented with a number of passes P with a progressively increasing threshold until a user-specified termination criterion is met. On each successive pass, DTO changes the topology of the decision space being searched as follows:

$$T_k = worst + \frac{C_{th}k}{P}(best - worst) \tag{13}$$

where, $k = 1, \ldots, P$ (no threshold applied for $k = 0$), where best and worst, respectively, are the best and worst overall fitnesses returned through pass k. Table 1 shows the values of the MGSA-PSO coefficients.

III. PROBLEM FORMULATION

In this section, the design configuration of the proposed circular polarized antenna element resonating at 28/38/48 GHz will be introduced. Then, the geometrical configuration of the suggested 8 × 4 array antenna is presented based on the designed antenna element as possible candidates for the future 5G mmWave base stations.

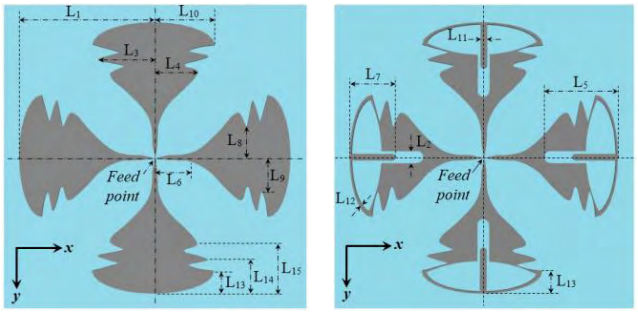

FIGURE 2. Configuration of the proposed bow-tie antennas, (a) Antenna design (Case I) and (b) Modified antenna design (Case II).

A. CONFIGURATION OF ONE ELEMENT ANTENNA DESIGN

Fig. 2(a) shows the geometry of the initial multiband antenna design, it consists of four radial stub-like bow-tie shapes with a tapering towards the outer end. The tapering ends are employed to increase the electrical length of the current path, which in turns widen the antenna impedance bandwidth and improving the return loss [27]. Furthermore, the bow-tie edges are sinusoidal modified to improve and resonate the antenna at different frequency bands [28]. The symmetrical structure of the antenna is considered to relatively stable the radiation patterns almost over the entire bandwidth, and improve the impedance matching.

In Fig. 2(b), the proposed bow-tie antenna is loaded with rounded T-shaped slot with a thin PCB copper line inside to have stabilized impedance response over the investigated frequency bands. The PCB copper line inside the slot, L_7, and rounded T-shaped are responsible for forcing the current to flow within the slot and changing the style of current distribution throughout all parts of the antenna, especially on the sides and edges. This leads to a significant increase in the electrical length of the current path. Thus, the increased electrical length of the bow-tie arm reduces the lower operation range to 28 GHz.

The modified bow-tie antenna has been printed on a low-loss Rogers® Duroid™ RT5880 with a 0.508 mm substrate thickness, relative permittivity $\varepsilon r = 2.2$, and loss tangent tan $\delta = 0.0009$ with a PEC ground plane. The antenna is fed by a SMA connector at the pool point of 4 arms to create a simple single-plane radiator that is easily integrated in low-profile or conformal geometries. The antenna dimensions of L_1, L_6, and L_9 is set to be 17.4 mm, 14.35 mm, and 3.21 mm respectively, however, other variables have to be optimized to fulfill the antenna design requirements.

B. 8 × 4 ARRAY ANTENNA DESIGN

Figs. 3(a) and 3(b) present the side and top view geometrical configurations of the proposed array antenna respectively. The array consists of 32-element distributed in an octagonal prism configuration with a ring radius $r = 10\ \lambda$, side length 4.2 λ, and height 16.8 λ. Each side includes four antenna elements with center-to-center distance of approximately 4.2 λ,

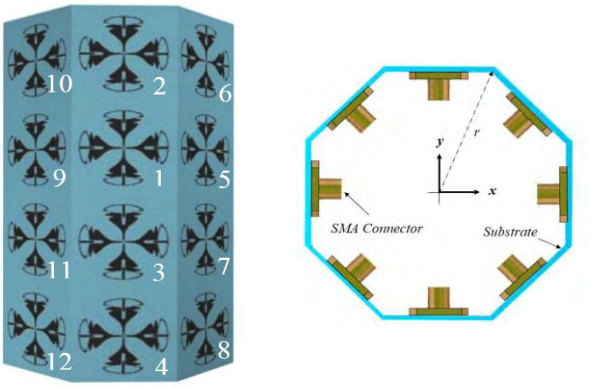

FIGURE 3. Array Antenna geometry for 5G Mobile Base station, (a) Side view and (b) Top view.

TABLE 2. The value of optimized dimensions (in millimeter).

Variable	Decision space		initial Value	Best Value	
	from	to		GSA-PSO	Modified GSA-PSO
L_2	1.3	4.4	1.3	2.95	2.63
L_3	3	14	3	10.26	7.21
L_4	3	10	3	6.81	5.40
L_5	6	13	6	9.21	8.71
L_7	3	12.5	3	6.47	5.82
L_8	3	8	3	3.82	3.17
L_{10}	6	15	6	8.16	8.70
L_{11}	1	2.5	1	1.90	2.05
L_{12}	0.2	2	0.5	0.92	1.03
L_{13}	2	5	2	3.11	2.708
L_{14}	3	6	3	4.27	3.98
L_{15}	4	8	4	6.50	6.77

where λ is the wavelength of 28 GHz. Initially, all elements are excited with the same amplitude and phase (1, 0°) which is called scenario #0. For beamforming synthesize, the amplitudes and phases were allowed to vary between 1 to 3 and from $-\pi$ to $+\pi$, respectively.

IV. RESULTS AND DISCUSSIONS

Firstly, the simulation and measured results of the optimized multiband circularly polarized antenna will be depicted, analyzed, and compared as a seed element for 5G base station. Then, the simulation results of the structured array antenna will be presented showing its capability for simultaneously synthesizing vertical and horizontal multi-beam patterns. To examine this capability, different scenarios will be considered in the azimuth and slant directions. Moreover, the performance of the proposed 5G base station will be introduced by using the metrics of total scan pattern and coverage efficiency.

A. SINGLE ELEMENT PERFORMANCE

To resonate the antenna at three CP operating frequency bands of 28, 38 and 48 GHz, the dimensions of the proposed antenna (Case II) were optimized by the modified GSA-PSO algorithm. The three sinusoidal curves' parameters of the bow-tie edge were optimized to reach the desired improvement at the assigned bands. It is found that, the first curve in the modified antenna can improve the matching at the low end of the band 28 GHz, however, the second curve is responsible to add another resonance near 48 GHz. The third curve is used to improve the match at 38 GHz [27]. Besides, a comparison between rounded solid bow-tie antenna (Case I) and slot-loaded bow-tie antenna (Case II) is executed to illustrate the effect of the rounded-T shaped slot with a thin microstrip line inside on the antenna characteristics.

The proposed antenna is analyzed completely using CST MWS [29] and linked with the optimization algorithm, Matlab-coded, to optimize the antenna dimensions. Accordingly, the following objective function is applied to minimize the return loss (S_{11}), axial ratio (AR), and maximizing the antenna gain (G) at the required operating frequency bands.

$$Obj_1 = \{\min[S_{11}(f) + AR(f)] + \max[G(f)]\}_{f=28,38,48\ GHz} \quad (14)$$

To prove the powerful and effectiveness of the modified MGSA-PSO algorithm on classical GSA-PSO, both algorithms were applied considering the same conditions with a swarm size of 20 and 500 iterations.

Fig. 4 shows the radiation characteristics of the modified bow-tie antenna and simultaneously illustrates the effect of the rounded-T shaped slot and sinusoidal curves on the antenna performance. It is clear that the rounded-T shaped slot with a thin PCB line inside has improved the matching resonance, gain, axial ratio, and radiation efficiency at the three frequency bands. Consequently, the modified antenna has effectively resonated at 28/38/48 GHz with an axial ratio less than 3dB.

It is clearly seen that, the MGSA-PSO algorithm markedly outperformed GSA-PSO and significantly enhanced the antenna properties. As shown in Fig. 4(a), better matching has been achieved by considering MGSA-PSO algorithm in different frequency bands to be −21.19, −20.89, and −25.49 at 28, 38, and 48 GHz, respectively, for the proposed antenna. Furthermore, optimizing the antenna dimensions by MGSA-PSO is significantly enhanced the antenna polarization with an axial ratio less than 3dB as shown in Fig 4 (b). Fig. 4 (c) illustrates the improvement in the realized gain, around 2 dB, using the modified MGSA-PSO. In addition, the radiation efficiency is increased by 15% on average as depicts in Fig. 4 (d). Table 2 list the optimized antenna parameters including the assigned decision space.

The surface current distribution over the proposed bow-tie antenna at resonance frequencies of 28/38/48 GHz is presented in Fig. 5. The simulated excited surface currents across the top, bottom, left and right bow-tie arms is balanced and approximately symmetric over the investigated frequency bands. As anticipated, the current flowing across the edges of the bow-tie is stronger in amplitude. The T-shaped slot-loaded bow-tie pattern forces the current to flow through the

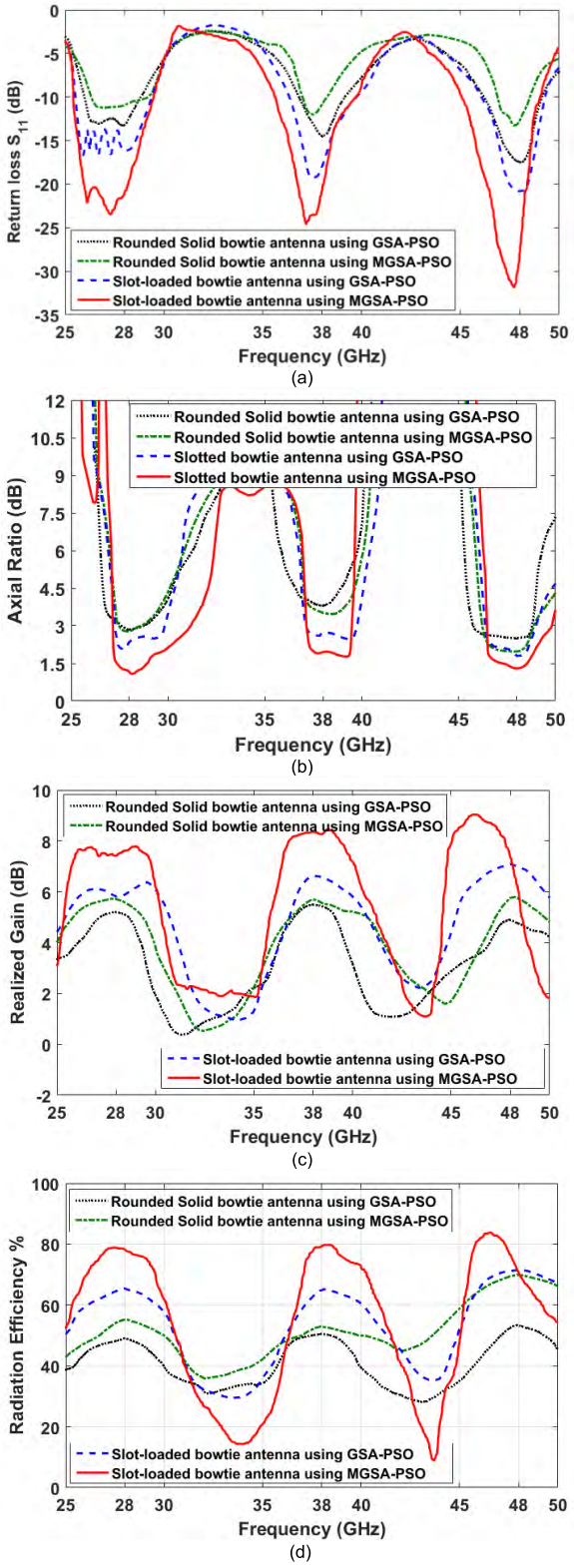

FIGURE 4. Comparison of the simulated results of different versions of the proposed antenna, (a) Return loss, (b) Gain, (c) Axial ratio, and (d) Radiation efficiency.

shaped modified geometry, increasing the electrical length of the proposed bow-tie antenna, especially at the lower band. At the first resonance mode (28 GHz) most current density is

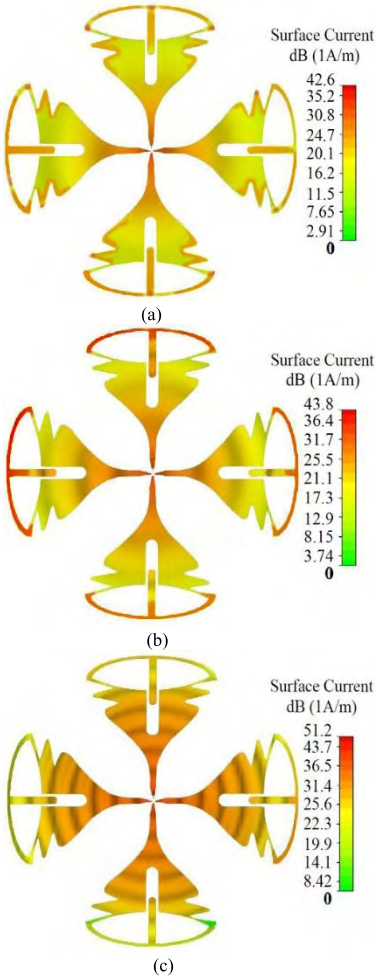

FIGURE 5. Simulated current distribution for the proposed antenna, (a) at 28 GHz (b) at 38 GHz (c) at 48 GHz.

concentrated around the feed point of the sub element bow-tie antenna, whereas the induced current density along the T-shaped slot-loaded bow-tie is getting larger as the operating frequency increases (i.e. at 38 GHz and 48 GHz excitation) to thus excite an additional mode. At the second and third resonant modes 38 GHz and 48 GHz, the current is less concentrated at the beginning of the radiating patch and moves to the T-shaped slot-loaded bow-tie of the antenna in asymmetrical manner. This clearly indicates the important effect of the four bow-tie strips to the proposed antenna's impedance matching. On the other hand, it can be noticed that on the fed line, a large current on the strip section exists with the same magnitude. Thus, the current density along the edges of the bow-ties has a great contribution to the bandwidth enhancement of an antenna.

Fig. 6 illustrates the simulated far field 3D radiation patterns of the single element antenna at different frequencies. The figure clearly depicts that the antenna has a broadside radiation pattern with 7.41 dB, 8.34 dB and 7.33 dB realized gain at 28, 38 and 48 GHz, respectively. It can be observed that the radiation pattern at 38 GHz has slightly split beams

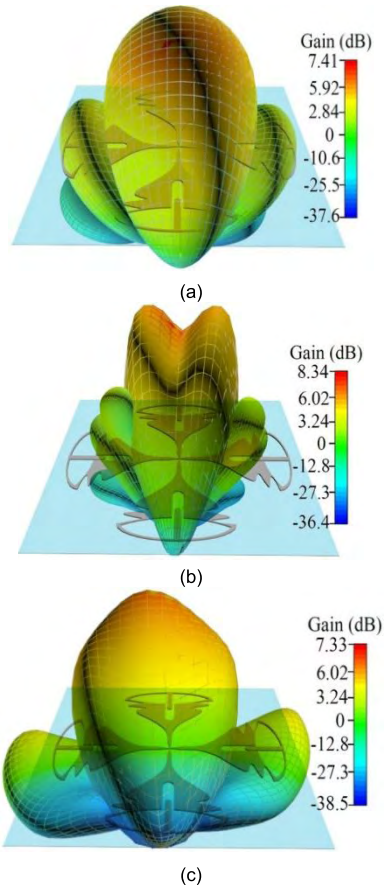

FIGURE 6. Simulated 3D radiation patterns for the proposed antenna at 28, 38 GHz, and 48 GHz, (a) at 28 GHz (b) at 38 GHz (c) at 48 GHz.

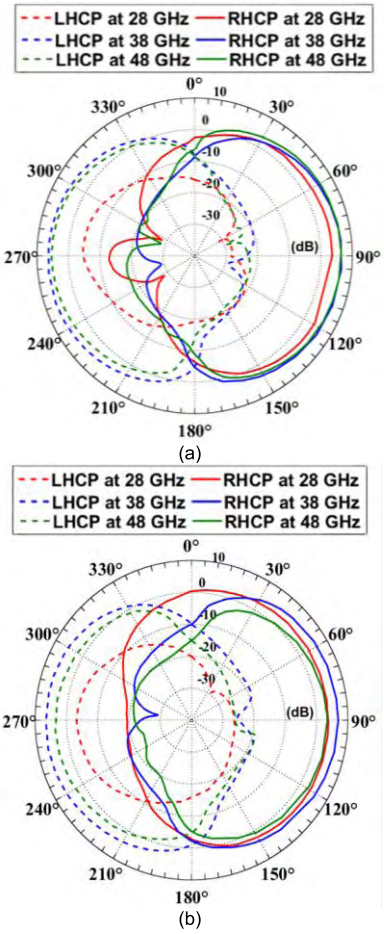

FIGURE 7. Simulated co-pol. and cross-pol. radiation patterns for the optimized antenna at 28/38/48 GHz. (a) x-y Plane and (b) x-z Plane.

at the broadside direction. Actually, by studding the radiation pattern around 38 GHz with frequency steps of 0.1 GHz, the split is slightly increased at f = 38.1 GHz and completely removed at 37.7 GHz. Furthermore, it should be noted that the realized gain at $\theta = 0°$ is found to be 8.3 dB at 37.7 GHz and decreased to 6.72 dB at 38.1 GHz which still high enough. This slight shift in the resonance frequency at 38 GHz has not any effect on the array beamforming performance.

Fig. 7 shows the calculated x-y plane and x-z plane co-polarization and cross-polarization radiation patterns for the proposed bow-tie antenna at various frequencies (28 GHz, 38 GHz, and 48 GHz). The figure clearly depicts approximately symmetric CP radiation patterns at different frequencies.

Fig. 8 shows a photograph of the fabricated triple-band CP antenna element which optimized by MGSA-PSO algorithm. The measurements of S_{11} and the realized antenna gain are presented in Figs. 9(a) and (b), respectively, and compared with the values produced using CST MWS. Overall, the simulations and experimental results are in good agreement, however, some discrepancies between simulated and measured results are observed, which are due to manufacturing tolerances and antenna assembly inaccuracy (connector soldering, etc.). As depicted in Fig. 9(a), the proposed antenna

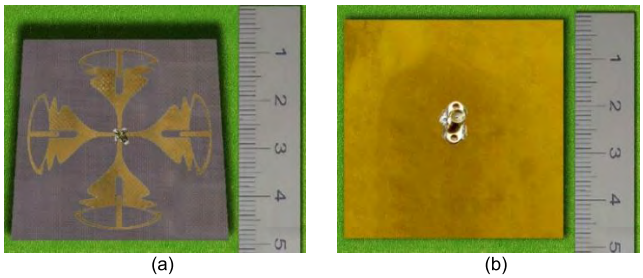

FIGURE 8. Photograph of fabricated one element antenna optimized by MGSA-PSO technique. (a) Top view and (b) Bottom view.

achieved good matching at all frequencies of operation with measured $S_{11} < -20$ dB, in addition, the realized gain is measured to be 7.82 dB, 8.39 dB and 7.7 dB at 28, 38 and 48 GHz, respectively, as shown in Fig. 9(b).

Fig. 10 shows a comparison between the normalized objective values of the GSA-PSO and MGSA-PSO algorithms plotted against iterations number. It can be observed that the MGSA-PSO algorithm outperformed the classical GSA-PSO algorithms by 22.2%. Furthermore, the modified GSA-PSO algorithm enhanced the convergence capability by 15% compared with the GSA-PSO algorithm.

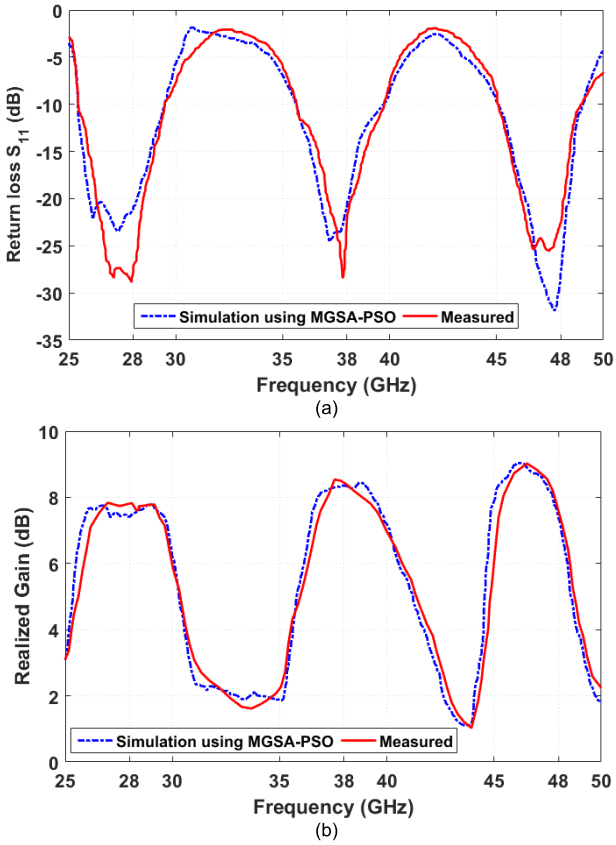

FIGURE 9. Comparison of the measured and simulated results for MGSA-PSO optimized bow-tie antenna. (a) Return loss and (b) Antenna gain.

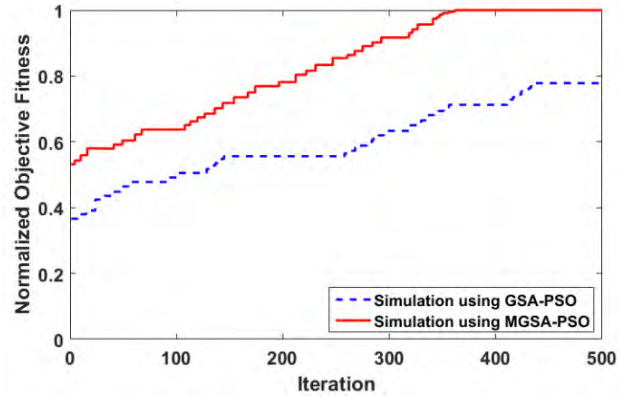

FIGURE 10. Comparison between the normalized objective values of the GSA-PSO and MGSA-PSO algorithms.

B. 8 × 4 ARRAY ANTENNA DESIGN

Firstly, the 8×4 array antenna distributed in the octagonal prism configuration are excited with the same amplitude and phase (1, 0°) to study the mutual coupling effect between the antenna elements. The simulated results of S-parameters for this scenario (#0) are presented in Fig. 11. It is apparent that the array antenna has a good impedance matching at the desired frequency bands of 28/38/48 GHz for S_{11} less than −20 dB with

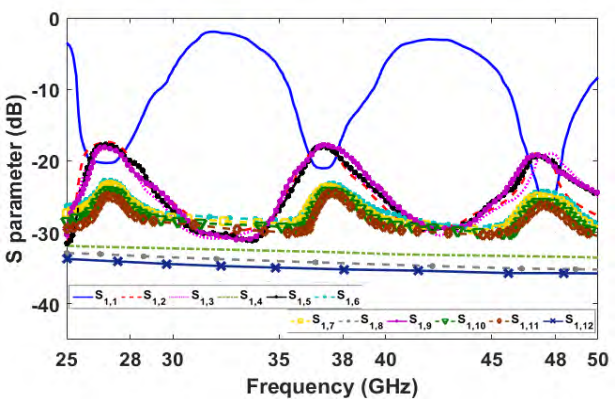

FIGURE 11. Simulated S-parameters of the proposed array antenna.

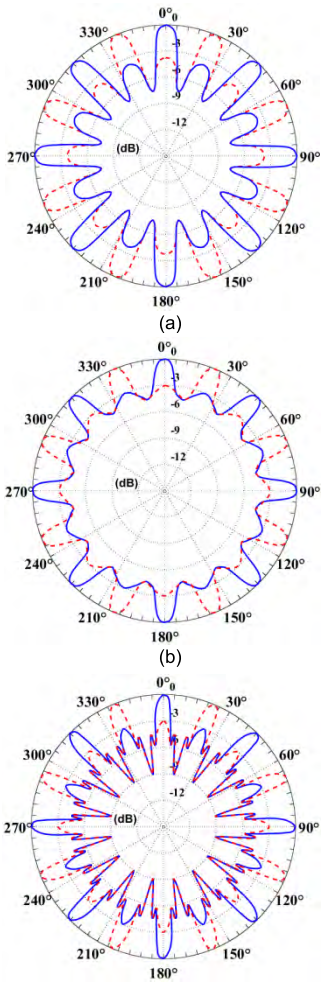

FIGURE 12. Normalized radiation pattern of the array antenna in x-y plane for scenarios #0 at different frequencies, (blue solid line – V.pol., red dashed line – H.Pol.), (a) at 28 GHz (b) at 38 GHz (c) at 48 GHz.

high isolation and weak mutual coupling between the array element ports gets below −16 dB throughout the operating bands. Fig. 12 shows the normalized radiation patterns of

TABLE 3. Descriptions of the environmental scenarios.

	Plane		Desired directions					Interferences' directions		
			φ_1	φ_2	φ_3	φ_4	φ_5	φ'_1	φ'_2	φ'_3
Scenario A1	V	$\theta_o = 90^o$	60°	180°	300°	---	---	30°	120°	240°
	H		30°	180°	240°	---	---	60°	120°	300°
Scenario A2	V.	$\theta_o = 135^o$	60°	180°	300°	---	---	30°	120°	240°
	H.		30°	180°	240°	---	---	60°	120°	300°
Scenario B1	V.	$\theta_o = 90^o$	0°	60°	120°	180°	300°	30°	240°	330°
	H.		30°	120°	180°	240°	330°	0°	60°	300°
Scenario B2	V.	$\theta_o = 135^o$	0°	60 °	120 °	180 °	300°	30°	240°	330°
	H.		30°	120°	180°	240°	330°	0°	60°	300°

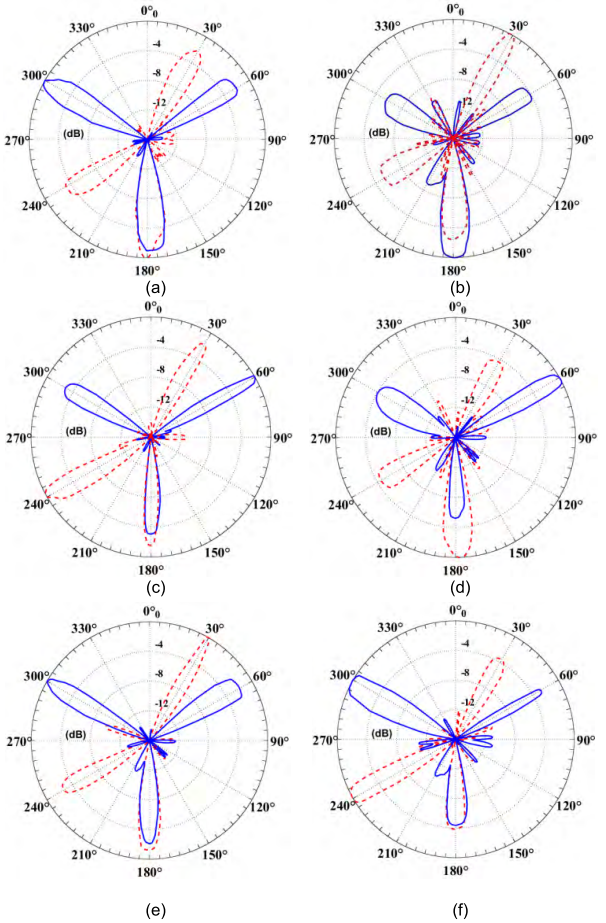

FIGURE 13. The radiation pattern of the base station for scenarios A1 and A2 at different frequencies, (blue solid line – V.pol., red dashed line – H.Pol.), (a) Scenario #A1 at 28 GHz (b) Scenario #A2 at 28 GHz (c) Scenario #A1 at 38 GHz (d) Scenario #A2 at 38 GHz (e) Scenario #A1 at 48 GHz (f) Scenario #A2 at 48 GHz.

the array antenna for scenario #0 in x-y plane at different frequencies. The same magnitude of E_θ and E_φ is observed with a relative rotation of 22.5°.

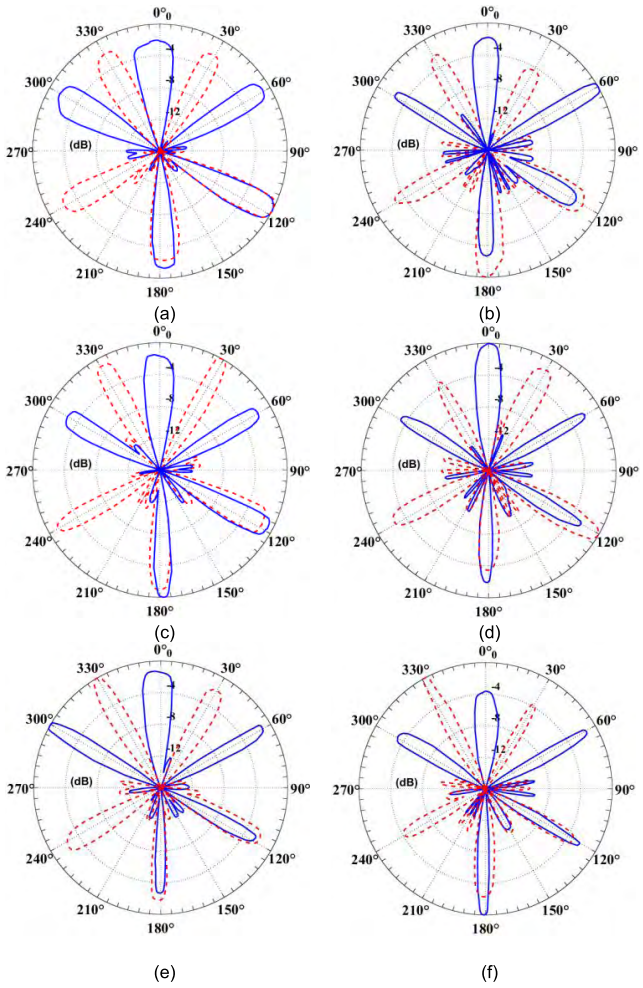

FIGURE 14. The radiation pattern of the base station for scenarios B1 and B2 at different frequencies, (blue solid line – V.pol., red dashed line – H.Pol.), (a) Scenario #B1 at 28 GHz (b) Scenario #B2 at 28 GHz (c) Scenario #B1 at 38 GHz (d) Scenario #B2 at 38 GHz (e) Scenario #B1 at 48 GHz (f) Scenario #B2 at 48 GHz.

Now, the capability of the base station for multi-beam pattern synthesize will be studied adopting directivity and polarization control in azimuth and slant directions. Therefore, MGSA-PSO as a powerful optimization technique is considered to optimize the feeding of array antenna elements with swarm size of 90 and 1000 iterations. In this target, different scenarios are considered in azimuth and slant directions at $\theta = 90°$ and $\theta = 135°$, respectively, considering multi desired and interferer users as shown in Table 3.

Scenarios (A1, B1) are considered for azimuthal direction ($\theta = 90°$). However, scenarios (A2, B2) are addressed the same directions in A1 and B1 but for slant angle of $\theta = 135°$ which is needed for directing the beams to directions not at the same plane with the base station. To fulfill the required beam patterns for all scenarios, a simple objective function rewards the antenna array is used for maximizing the output field toward the desired signals and minimizing the total output field in the direction of the interfering signals

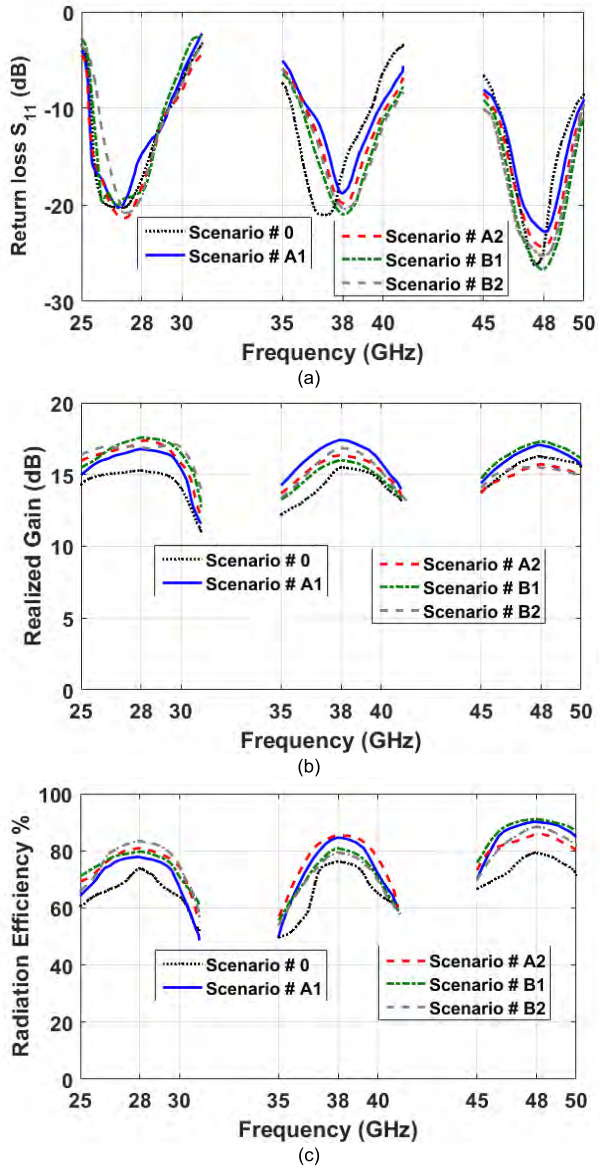

FIGURE 15. Comparison of radiation characteristics of the proposed array antenna for different scenarios, (a) Return loss (b) Antenna gain (c) Radiation efficiency.

considering the field polarization.

$$Obj_2 = \sum_{i=1}^{N} |E_\theta(\varphi_i)| + \sum_{j=1}^{M} |E_\varphi(\varphi_j)| - \sum_{k=1}^{P} |E_\theta(\varphi_k)| - \sum_{l=1}^{Q} |E_\varphi(\varphi_l)| \quad (15)$$

where E_θ and E_φ are the vertical and horizontal field components, respectively. The constants N and P represents the number of desired and interferer users who covered with vertically polarized signal (V-pol.), whereas M and Q represent the number of desired and interferer users who covered horizontally (H-pol.). In our analysis, we take $N = M = P = Q = 3$ for scenarios A1 and A2. But for scenarios B1 and B2, the number of desired users is considered to be $N = M = 5$, and the number of interferer users' $P = Q = 3$.

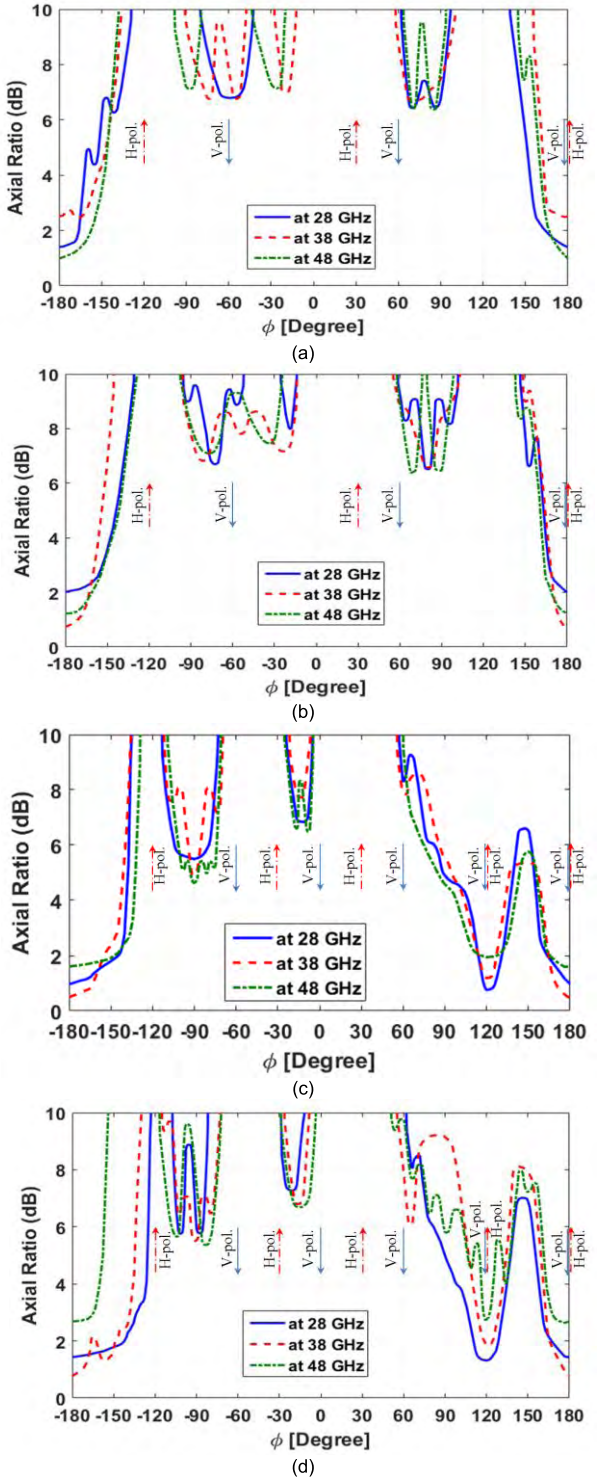

FIGURE 16. Axial ratio of the proposed array antenna versus φ-angle for different scenarios at 28/38/48 GHz (a) scenario A1 (b) scenario A2 (c) scenario B1 (d) scenario B2.

Although all antenna elements are CP, but with the appropriate feeding assigned by the optimizer to fulfil the objective function, the E_θ and/or E_φ components can be maximized and/or minimized in the desired directions. Fig. 13 and Fig. 14 illustrate the optimized beam patterns for scenarios

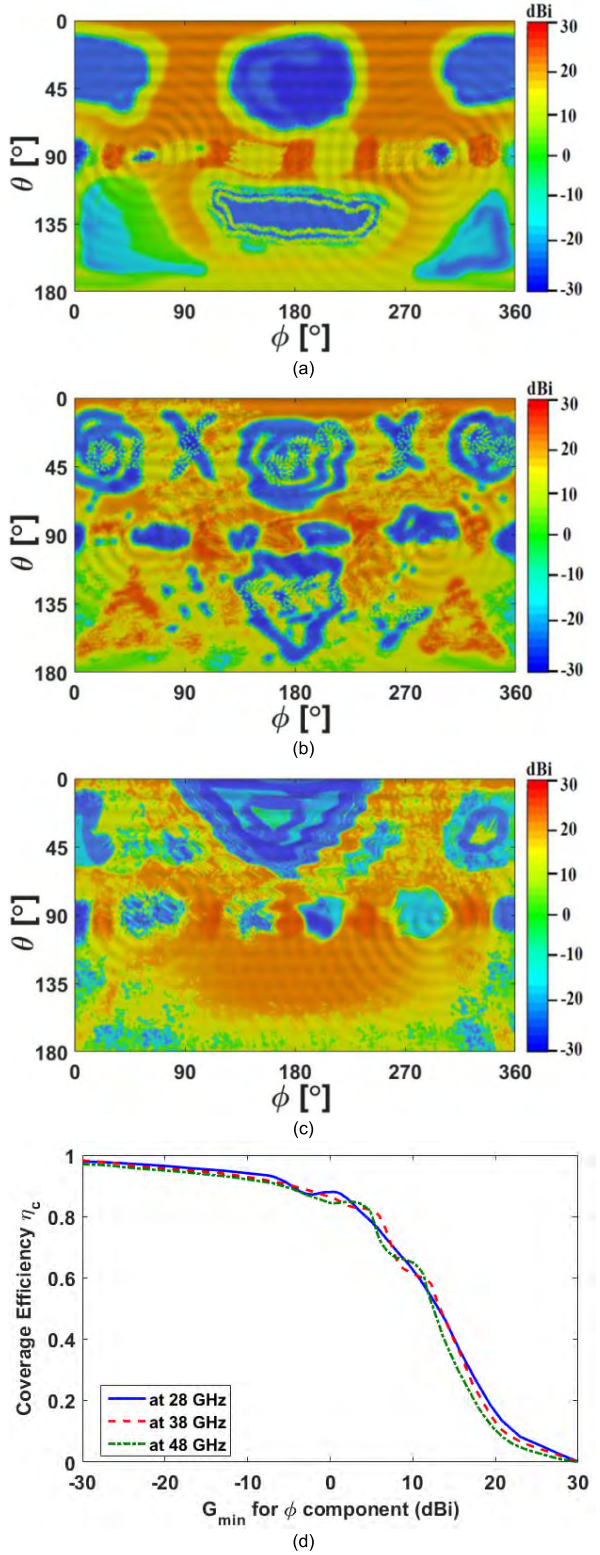

FIGURE 17. Total scan patterns and coverage efficiency for phased array antenna at different frequency bands (H-pol. Scenario B1). (a) Total scan patterns at 28 GHz (b) Total scan patterns at 38 GHz (c) Total scan patterns at 48 GHz (d) Coverage efficiency comparison.

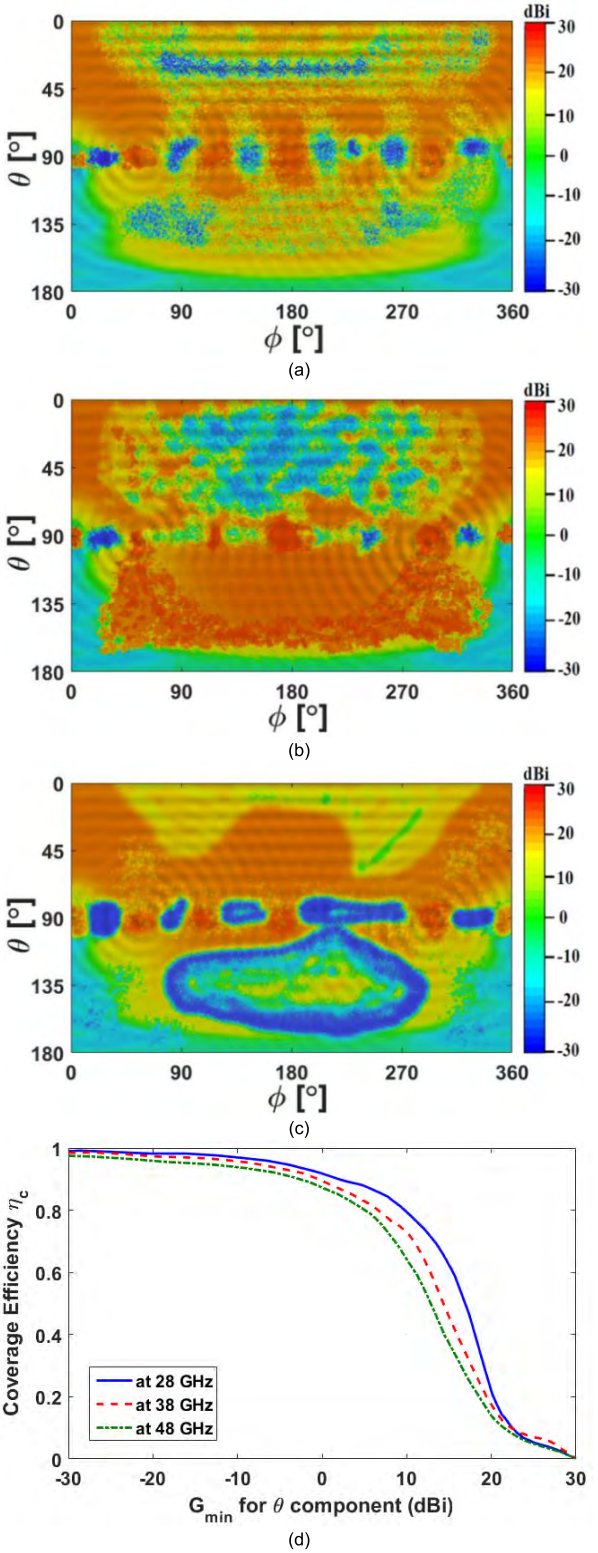

FIGURE 18. Total scan patterns and coverage efficiency for phased array antenna at different frequency bands (V-pol. Scenario B1). (a) Total scan patterns at 28 GHz (b) Total scan patterns at 38 GHz (c) Total scan patterns at 48 GHz (d) Coverage efficiency comparison.

(A1 and A2) and scenarios (B1 and B2), respectively, at 28/38/48 GHz frequency bands. Compared to Fig. 12, the figures show the capability of the designed array antenna to direct the maximum field of E_θ and/or E_φ towards the direction of signal of interest (SOI) either in the azimuth or slant planes while placing deeper nulls towards

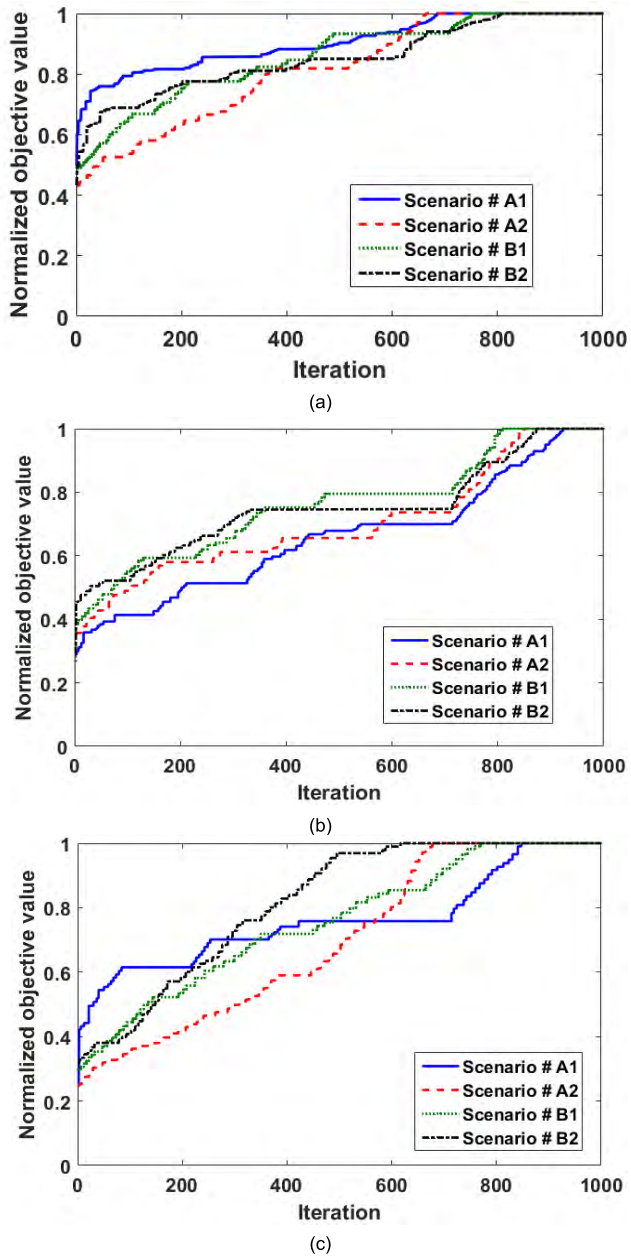

FIGURE 19. Comparison between the normalized objective values of the MGSA-PSO algorithm for different scenarios at (a) 28 GHz (b) 38 GHz (c) 48 GHz.

the angles of signal not of interest (SNOI). Additionally, the figures indicate the ability of octagonal prism antenna array to serve two terminals even if the angle-of-arrival difference between them is 0° at 28/38/48 GHz. Moreover, the results show the high efficiency of the MGSA-PSO algorithm for beamforming applications.

Fig. 15(a) depicts the return loss results of the array antenna for different scenarios. It is found that, the matching resonance at triple frequency bands are slightly affected due to the change in the feeding phases and amplitudes from scenario to another, but for all cases it is still under −18 dB. Furthermore, a realized gain not less than 16 dB has been obtained for different scenarios, whereas, the array antenna has achieved a realized gain, on average, equal to 16.78 dB, 16.42 dB, and 16.36 dB at 28/38/48 GHz, respectively, as shown in Fig. 15(b). Besides, acceptable radiation efficiencies of 79.12%, 81.5%, and 85.25% are obtained, on average, at operating frequencies of 28 GHz, 38 GHz, and 48 GHz, respectively.

Fig. 16 shows the axial ratio versus angels in x-y plane for different scenarios at 28/38/48 GHz. The figure indicates that, the array antenna served as V/H polarized array antenna in certain directions and as circular polarized in other directions based on the assumed scenario. For example, in scenario B1, the axial ratio is found to be less than 3dB at $\varphi = 120°$ and $\varphi = 180°$, whereas two users are located at the same position (one of them will covered with vertical polarized beam pattern and the second with horizontal polarized beam pattern) as assumed in Table 3. However, the base station is served as V/H linear polarized array antenna at other directions of 0°, 30°, 60°, and 240°.

In brief, distributing the proposed 32-element in an octagonal prism configuration achieved good results in all antenna properties such as return loss, realized gain, radiation efficiency and axial ratio.

Now, scenario B1 will be considered as an example to study the coverage efficiency (η_c) of the proposed array antenna as a function of minimum received gain (G_{min}). Figs. 17 and 18 show the total scan pattern and coverage efficiency simulated results of scenario B1 for H-pol. And V-pol. beam-patterns at 28, 38 and 48 GHz, respectively. The figures indeed illustrate hot and cold spots at the desired and interferer directions, respectively, as assumed in Table 3 for different frequencies. In Fig. 17(d), the coverage efficiency is approximately the same for different operating frequencies. However, the coverage efficiency shown I Fig. 18 (d) has significantly affected by the operating frequency which dropped to 83.85 %, 76.9 %, and 72 % when the threshold gain exceeds 8 dBi for array antenna at 28, 38, and 48 GHz, respectively.

Lastly, the convergence capability of the MGSA-PSO for muti-beam patterns synthesize is studied for different scenarios as shown in Fig. 19. The figure presents a comparison between the normalized objective values of different scenarios at operating frequencies of 28/38/48 GHz. It is clear that, all scenarios at different frequencies are converged before realizing the assigned maximum number of iterations.

V. CONCLUSION

In this paper, a novel design of tri-band multi-polarized array antenna for 5G mmWave cellular mobile networks is presented. The fundamental element array antenna is designed to resonate at 28/38/48 GHz with gain value more than 7.5 dB and axial ratio less than 3 dB at each band. The performance of array antenna to form simultaneously multiple V/H directional beams adopting the polarization and directivity control is introduced for different scenarios. The matching resonance at different frequency bands are still under −18 dB for different scenarios with an acceptable realized

gain of 16.6 dB on average. A modified version of GSA-PSO is introduced to obtain a truly optimum design of antenna element, and beamforming synthesize. The obtained results reveals that the MGSA-PSO optimization technique has the ability to enhance the global search capability of the classical GSA-PSO method and effectively improves its convergence capability. The promising results show that the proposed design has good performance in terms of S-parameters, antenna gain, efficiency, and beamforming characteristics in the entire operation bands, which is fitting the need of mmWave 5G communications.

REFERENCES

[1] X. Wei, K. Zheng, and X. S. Shen, Eds. *5G Mobile Communications*. Cham, Switzerland: Springer, 2017.
[2] A. Ghosh, "The 5G mmWave radio revolution," *Microw. J.*, vol. 59, no. 9, pp. 3–10, 2016.
[3] T. S. Rappaport *et al.*, "Millimeter wave mobile communications for 5G cellular: It will work!" *IEEE Access*, vol. 1, pp. 335–349, 2013.
[4] M. Elkashlan, T. Q. Duong, and H.-H. Chen, "Millimeter-wave communications for 5G: Fundamentals: Part I [guest editorial]," *IEEE Commun. Mag.*, vol. 52, no. 9, pp. 52–54, Sep. 2014.
[5] M. Elkashlan, T. Q. Duong, and H.-H. Chen, "Millimeter-wave communications for 5G—Part 2: Applications," *IEEE Commun. Mag.*, vol. 53, no. 1, pp. 166–167, Jan. 2015.
[6] A. Gupta and E. R. K. Jha, "A survey of 5G network: Architecture and emerging technologies," *IEEE Access*, vol. 3, pp. 1206–1232, 2015.
[7] J. Curtis, H. Zhou, P. Hisayasu, A. Sarkar, and F. Aryanfar, "MM-wave radio, a key enabler of 5G communication," in *Proc. IEEE 16th Topical Meeting Silicon Monolithic Integr. Circuits RF Syst. (SiRF)*, Austin, TX, USA, Jan. 2016, pp. 1–3.
[8] *Use of Spectrum Bands Above 24 GHz for Mobile Radio Services*, document GN Docket 14–177, Notice Proposed Rulemaking, FCC Record 89A1, Jul. 2016.
[9] A. I. Sulyman, A. T. Nassar, M. K. Samimi, G. R. MacCartney, Jr., T. S. Rappaport, and A. Alsanie, "Radio propagation path loss models for 5G cellular networks in the 28 GHz and 38 GHz millimeter-wave bands," *IEEE Commun. Mag.*, vol. 52, no. 9, pp. 78–86, Sep. 2014.
[10] J. Zhang, X. Ge, Q. Li, M. Guizani, and Y. Zhang, "5G millimeter-wave antenna array: Design and challenges," *IEEE Wireless Commun.*, vol. 24, no. 2, pp. 106–112, Apr. 2017.
[11] T. Kim, J. Park, J.-Y. Seol, S. Jeong, J. Cho, and W. Roh, "Tens of Gbps support with mmWave beamforming systems for next generation communications," in *Proc. IEEE GLOBECOM*, Atlanta, GA, USA, Dec. 2013, pp. 3685–3690.
[12] W. Roh *et al.*, "Millimeter-wave beamforming as an enabling technology for 5G cellular communications: Theoretical feasibility and prototype results," *IEEE Commun. Mag.*, vol. 52, no. 2, pp. 106–113, Feb. 2014.
[13] E. Turgut and M. C. Gursoy, "Coverage in heterogeneous downlink millimeter wave cellular networks," *IEEE Trans. Commun.*, vol. 65, no. 10, pp. 4463–4477, Oct. 2017.
[14] K. Komiya, K. Nishimori, K. Cho, and T. Hori, "Proposal of SDMA configuration adopting directivity and polarization control," *Electron. Commun. Jpn (Commun.)*, vol. 90, no. 2, pp. 33–45, 2007.
[15] K. R. Mahmoud, R. Bansal, M. I. El-Adawy, S. H. Zainud-Deen, and S. M. M. Ibrahem, "Performance of a circular crossed-dipole array for SDMA configuration adopting directivity and polarization control using particle swarm optimization algorithm," *Int. J. RF Microw. Comput.-Aided Eng.*, vol. 19, no. 1, pp. 50–59, 2009.
[16] O. M. Haraz, M. M. Ashraf, and S. Alshebili, "8×8 Patch antenna array with polarization and space diversity for future 5G cellular applications," in *Proc. Int. Conf. IEEE Inf. Commun. Technol. Res. (ICTRC)*, May 2015, pp. 258–261.
[17] S.-T. Liu, Y.-W. Hsu, and Y.-C. Lin, "A dual polarized cavity-backed aperture antenna for 5G mmW MIMO applications," in *Proc. IEEE Int. Conf. Microw., Commun., Antennas Electron. Syst. (COMCAS)*, Nov. 2015, pp. 1–5.
[18] H. Chu and Y.-X. Guo, "A filtering dual-polarized antenna subarray targeting for base stations in millimeter-wave 5G wireless communications," *IEEE Trans. Compon., Packag., Manuf. Technol.*, vol. 7, no. 6, pp. 964–973, Jun. 2017.
[19] B. Sadhu *et al.*, "A 28 GHz 32-element phased-array transceiver IC with concurrent dual polarized beams and 1.4 degree beam-steering resolution for 5G communication," in *IEEE Int. Solid-State Circuits Conf. (ISSCC) Dig. Tech. Papers*, San Francisco, CA, USA, Feb. 2017, pp. 128–129.
[20] W. Hong, S.-T. Ko, Y. Lee, and K.-H. Baek, "Multi-polarized antenna array configuration for mmWave 5G mobile terminals," in *Proc. Int. Workshop Antenna Technol. (iWAT)*, Seoul, South Korea, Mar. 2015, pp. 60–61.
[21] K. R. Mahmoud and A. M. Montaser, "Design of dual-band circularly polarised array antenna package for 5G mobile terminals with beam-steering capabilities," *Microw., Antennas Propag.*, vol. 12, no. 1, pp. 29–39, Jan. 2017.
[22] E. Rashedi, H. Nezamabadi-Pour, and S. Saryazdi, "GSA: A gravitational search algorithm," *J. Inf. Sci.*, vol. 179, no. 13, pp. 2232–2248, 2009.
[23] S. Mirjalili and S. Z. M. Hashim, "A new hybrid PSOGSA algorithm for function optimization," in *Proc. Int. Conf. Comput. Inf. Appl.*, Dec. 2010, pp. 374–377.
[24] M. Hussein, K. R. Mahmoud, M. F. O. Hameed, and S. S. A. Obayya, "Optimal design of vertical silicon nanowires solar cell using hybrid optimization algorithm," *J. Photon. Energy*, vol. 8, no. 2, p. 022502, 2017.
[25] R. A. Formato. (2012). "Dynamic threshold optimization—A new approach?" pp. 1–17. [Online]. Available: https://arxiv.org/abs/1206.0414
[26] A. Ratnaweera, S. K. Halgamuge, and H. C. Watson, "Self-organizing hierarchical particle swarm optimizer with time-varying acceleration coefficients," *IEEE Trans. Evol. Comput.*, vol. 8, no. 3, pp. 240–255, Jun. 2004.
[27] O. Yurduseven, D. Smith, and M. Elsdon, "Printed slot loaded bowtie antenna with super wideband radiation characteristics for imaging applications," *IEEE Trans. Antennas Propag.*, vol. 61, no. 12, pp. 6206–6210, Dec. 2013.
[28] R. G. Pierce, A. J. Blanchard, and R. M. Henderson, "Broadband planar modified aperture bowtie antenna," *IEEE Antennas Wireless Propag. Lett.*, vol. 12, pp. 1432–1435, 2013.
[29] *Computer Simulation Technology Microwave Studio (CST MWS)*. Accessed: 2017. [Online]. Available: http://www.cst.com

KORANY R. MAHMOUD received the B.S. and M.S. degrees in communications and electronics engineering from Helwan University in 1998 and 2003, respectively, and the Ph.D. degree from Helwan University in collaboration with the University of Connecticut, USA, in 2008. Since 2012, he has been a Consultant with the Research and Development Department, National Telecommunications Regulatory Authority, Egypt. He was also a Post-Doctoral Fellow with the Center for Photonics and Smart Materials, Zewail City, Egypt. He is currently an Associate Professor with the Department of Communications and Electronics Engineering in the same Faculty. His current research interests include mmWave and optical antenna designs and optimization techniques.

AHMED M. MONTASER was born in Luxor, Egypt, in 1981. He received the B.S. and M.S. degrees in communications and electronics engineering from South Valley University, Aswan, Egypt, in 2003 and 2009, respectively, and the Ph.D. degree from Mansoura University, Egypt, in 2013. He is currently an Assistant Professor with the Department of Communication and Electronics, Sohag University, Sohag, Egypt. He served as an editor/reviewer of many international journals. His current research interests include antenna design, multiband PIFA for mobile phone communications, computational electromagnetic, body-centric wireless communications, mm-wave antennas, and multiple antennas–user interactions.